Nanoscale

PAPER

View Article Online
View Journal | View Issue

Cite this: *Nanoscale*, 2014, **6**, 3296

Cauliflower-like SnO_2 hollow microspheres as anode and carbon fiber as cathode for high performance quantum dot and dye-sensitized solar cells†

Veerappan Ganapathy,‡[a] Eui-Hyun Kong,‡[b] Yoon-Cheol Park,[c] Hyun Myung Jang*[b] and Shi-Woo Rhee*[a]

Received 25th October 2013
Accepted 13th December 2013

DOI: 10.1039/c3nr05705d

www.rsc.org/nanoscale

Cauliflower-like tin oxide (SnO_2) hollow microspheres (HMS) sensitized with multilayer quantum dots (QDs) as photoanode and alternative stable, low-cost counter electrode are employed for the first time in QD-sensitized solar cells (QDSCs). Cauliflower-like SnO_2 hollow spheres mainly consist of 50 nm-sized agglomerated nanoparticles; they possess a high internal surface area and light scattering in between the microspheres and shell layers. This makes them promising photoanode material for both QDSCs and dye-sensitized solar cells (DSCs). Successive ionic layer adsorption and reaction (SILAR) method and chemical bath deposition (CBD) are used for QD-sensitizing the SnO_2 microspheres. Additionally, carbon-nanofiber (CNF) with a unique structure is used as an alternative counter electrode (CE) and compared with the standard platinum (Pt) CE. Their electrocatalytic properties are measured using electrochemical impedance spectroscopy (EIS), cyclic voltammetry (CV), and Tafel-polarization. Under 1 sun illumination, solar cells made with hollow SnO_2 photoanode sandwiched with the stable CNF CE showed a power conversion efficiency of 2.5% in QDSCs and 3.0% for DSCs, which is quite promising with the standard Pt CE (QDSCs: 2.1%, and DSCs: 3.6%).

1. Introduction

In the last decade, solar cells have been developed into a most interesting alternative to the energy demand of the world. Among solar cells, dye-sensitized solar cells (DSCs) and quantum dot-sensitized solar cells (QDSCs) emerged as a viable substitute to solid state silicon solar cells because of their low cost, simple cell structure and promising energy conversion efficiency.[1–5] In QDSCs, a narrow band-gap semiconductor such as quantum dots (QDs) has been widely used for photoanode sensitization instead of the expensive ruthenium dye. Due to an easy band gap tuning by varying the particle size and its higher absorption properties makes QDs very promising candidates for efficient light harvesting materials in this type of solar cells.[4–8]

Though a record efficiency higher than 12.0% was achieved using randomly oriented TiO_2 films in DSCs, further improvement with TiO_2 is still difficult due to its slow electron transport and higher charge recombination.[9,10] Many groups have already suggested using alternative metal oxides such as SnO_2, ZnO, Nb_2O_5, $BaSnO_3$, and Zn_2SnO_4.[11–15] Among them SnO_2 possesses some unique properties such as high electron mobility (100–200 $cm^2\ V^{-1}\ S^{-1}$) and importantly its conduction band edge position is more positive than TiO_2.[5,11,16,17] Commonly used randomly oriented nanoparticle photoanodes possess grain boundaries at the interparticle connection and the disordered pore structure. In the recent progress for development of DSCs for higher photovoltaic performance, ordered nanostructures such as one-dimensional (1D) nanostructures, coral like structures are used to increase electron transport and to reduce recombination.[18–21] Nevertheless the 1D structure has a small surface area and thus results in low efficiency. All the above DSC reports suggest that the ordered high surface SnO_2 photoanode can be a vital photoanode material, but their potential was never fully utilized in QDSCs.[11,16,22,23] It is well accepted that just increasing the surface area does not give a high efficiency photoanode. It also requires a densely packed microstructure and bi-functional property for light harvesting. Furthermore, the light scattering property can give high photo conversion efficiency in DSCs.[24,25] Due to the positive conduction band edge

[a]*Department of Chemical Engineering, Pohang University of Science and Technology (POSTECH), Pohang 790-784, Korea. E-mail: srhee@postech.ac.kr*

[b]*Department of Materials Science and Engineering, and Division of Advanced Materials Science, Pohang University of Science and Technology (POSTECH), Pohang 790-784, Korea. E-mail: hmjang@postech.ac.kr*

[c]*Research Institute of Industrial Science and Technology (RIST), Pohang 790-784, Korea*

† Electronic supplementary information (ESI) available: Experimental details, XRD, SEM-EDS, UV-vis spectra and photovoltaic parameters of devices. See DOI: 10.1039/c3nr05705d

‡ V. Ganapathy and E.-H. Kong contributed equally to this work.

position of SnO_2, electron injection from low band gap QDs can be facilitated like PbS, Sb_2S_3, $CuInS_2$.[26–28] In this regard, SnO_2 is a suitable photoanode material, which could facilitate the efficient electron injection and collection. However the conversion efficiency of SnO_2 photoanode is still strangely poor in DSCs, although it shows great promise in solid-state DSCs and QDSCS.[18,23] To further improve the photovoltaic property, multilayer QDs (CdS/CdSe/ZnS) were sensitized on SnO_2 and reported lately.[22] Due to weakening of quantum dots in iodine redox electrolyte, aqueous polysulfide electrolyte (S^{2-}/S_x^{2-}) was used to improve the performance with platinum (Pt) counter electrode (CE).[29] However, the device showed low efficiency and fill factor (FF) due to the poor catalytic activity, and long term stability of Pt in sulfur electrolyte is still in doubt. To overcome these drawbacks, several groups have attempted to replace Pt with CuS, CoS, Cu_2S, and carbon materials.[30–33] Carbon material has a promising potential due to its excellent corrosion resistance, low cost and low temperature processability. Most reported carbon CE needs a high temperature process (400 °C) to remove the organic binder used to make the paste.[34,35] Carbon materials with edge planes possess more catalytic sites for the reduction reaction in photovoltaic applications.[34,36]

In this regard, we report the use of hydrothermally synthesized cauliflower-like SnO_2 hollow microspheres (SnO_2-HMS) as a photoanode instead of the standard TiO_2, and additionally the use of highly stable and low temperature processed carbon-nanofiber (CNF) CE to replace traditional Pt CE for highly efficient and stable QDSCs and DSCs.

2. Experimental

2.1. Fabrication of QDSCs and DSCs

Hydrothermal synthesized SnO_2-HMS was prepared into a highly viscous paste and screen-printed onto FTO glass. Simultaneously CNF CE was prepared from the thick paste of commercial CNF powder mixed with carboxy-methyl cellulose. The paste was coated onto the FTO glass *via* a doctor blade technique. The sintered SnO_2 electrodes were cooled down to 80 °C and immediately immersed in a 0.3 mM solution of N719 dye in absolute ethanol for 24 h. Dye-adsorbed SnO_2-HMS electrodes were removed from the dye solution, rinsed with absolute ethanol, and then dried with nitrogen gas. The N719-sensitized SnO_2 photoanode and CE were sandwiched using a 60 μm-thick surlyn spacer (surlyn-1702, Dupont). The iodine electrolyte was introduced into the sandwiched cell through a hole drilled in the CE, and the hole was then sealed with a surlyn spacer and cover glass. The electrolyte was composed of 0.5 M butylmethyl-imidazolium iodide, 0.06 M I_2, 0.5 M 4-*tert*-butylpyridine in an acetonitrile solvent.

A successive ionic layer adsorption and reaction (SILAR) technique was employed to deposit the CdS QDs on the SnO_2 film.[37] Two separate solutions were prepared: 0.1 M $Cd(NO_3)_2$ in ethanol and 0.1 M Na_2S in methanol. Working electrodes were immersed into the Cd^{2+} solution and the S^{2-} solution successively for 2 min each. After dipping into one solution, the electrodes were washed with ethanol and methanol to remove the excess of each precursor. The number of the SILAR cycles was optimized to be 6 in our experimental conditions. Then, the CdSe QDs were deposited on the CdS QD-sensitized SnO_2 anodes using chemical bath deposition (CBD). SnO_2/CdS films were dipped in an aqueous solution containing $Cd(SO_4)$–Na_2SeSO_3–$N(CH_2COONa)_3$ = 80 mM : 80 mM : 160 mM at 10 °C for 12 h. The Na_2SeSO_3 aqueous solution was prepared by refluxing Se (0.5 M) in an aqueous solution of Na_2SO_3 (0.6 M) at 120 °C for 7 h. The CdSe QD-sensitized films were rinsed with deionized water. Then, the films were dipped again in 0.5 M aqueous Na_2SeSO_3 solution at 70 °C for 30 min to remove residual Cd^{2+} ions, which otherwise could cause the formation of the CdS QDs on the deposited CdSe QDs.[38] ZnS was finally deposited on top of the sensitized films through the SILAR process. For the ZnS passivation, two separate solutions were used: 0.1 M aqueous $Zn(NO_3)_2$, and 0.1 M aqueous Na_2S. Two SILAR cycles were used. The polysulfide electrolyte was composed of 1 M S and 1 M Na_2S in deionized water. Simultaneously TiO_2 photoelectrodes were prepared with similar experimental conditions and assembled with either CNF or Pt CE for both QDSCs and DSCs. Detailed experimental methods are presented in the ESI.†

3. Results and discussion

Fig. 1 shows a schematic diagram of QDSCs composed of SnO_2 photoanode and CNF CE sandwiched and filled with sulfur redox electrolyte. Inside the schematic diagram, the electron transfer from quantum dot into SnO_2-HMS and reduction reaction mechanism in CNF CE is shown. Cauliflower-like SnO_2-HMS was synthesized by a two step process. SnO_2 spheres were prepared by a chemically induced self-assembly reaction of aqueous sucrose–$SnCl_4$ solution under hydrothermal conditions.[39] And the resulting black precipitate yielded carbon/SnO_2 spheres. Subsequently the carbon/SnO_2 spheres were sintered at 600 °C for 3 h to remove carbon and white color cauliflower-

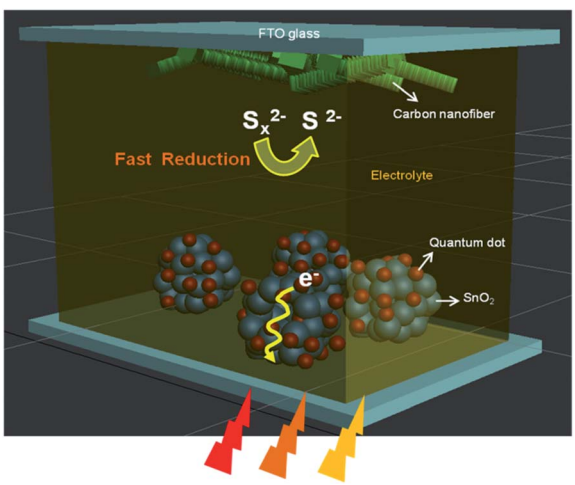

Fig. 1 Schematic diagram showing the device architecture composed of SnO_2 photoanode and carbon-nanofiber counter electrode with sulfur redox electrolyte. The electron transport from quantum dots into SnO_2-HMS and the reduction reaction mechanism in carbon-nanofiber counter electrode are also shown.

like SnO_2-HMS was formed. Fig. 2 shows the unique morphologies of the SnO_2-HMS surface and cross sectional SEM images. From the SEM images, it is clearly evident that the hollow spheres is composed of aggregated small SnO_2 nanoparticles with diameter of ~50 nm. The hollow SnO_2 structures were formed due to removal of residual carbon in the SnO_2 spheres. As shown in Fig. 2a and b, most of the SnO_2 spheres are spherical in shape with a size variation from 500 nm–2 μm. A cross-sectional SEM image (Fig. 2c) shows the screen printed SnO_2-HMS on FTO glass with uniform film thickness. Multilayer quantum dots (CdS/CdSe/ZnS) were uniformly sensitized on top of the SnO_2-HMS by SILAR (Fig. 2d) for efficient light harvesting. To further confirm the QD distribution on SnO_2-HMS, SEM-EDS was measured for the bare SnO_2/TiO_2 and QD sensitized SnO_2/TiO_2 photoanode (Fig. S1b and c†). XRD was measured for the SnO_2-HMS after 600 °C sintering and it shows a highly crystalline rutile phase (Fig. S1a†). Likewise, strong sharp peaks were obtained at 2θ of 25.2, 33.5, 37.5, 52.0, and 54.1°, corresponding to a crystalline rutile phase with orientations of (111), (101), (200), (211), and (220), respectively.

The surface and cross-sectional morphological structures of the unique CNF nanostructures were measured using SEM and TEM analysis (Fig. 3). Doctor bladed CNF on FTO substrates were given in Fig. 3a and b. The CNF CE formed on FTO glass composed of carbon fibers with size ranging from several micrometers in length and more than 100 nm in diameter. The CNF used in this work possesses a good nanostructure which is beneficial for the catalytic reduction reaction. The antler like structures in the edges of the fibers can act as catalytic sites in CE (Fig. 3c). Carbon materials with more edge planes can act as a highly effective CE.[34,36] The CNF film made on the FTO glass is uniform with a film thickness of ~11 μm (Fig. 3b).

To further highlight the promising properties of SnO_2-HMS, the diffuse reflectance was measured (Fig. S2†). In our previous

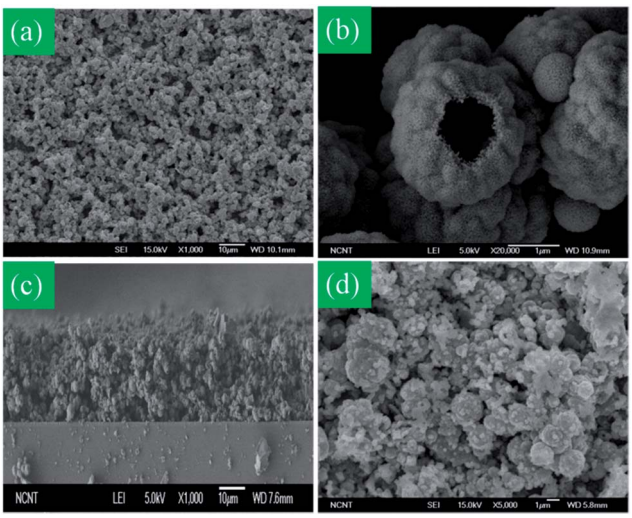

Fig. 2 SEM surface morphology of the SnO_2-HMS powders and films deposited on FTO glass substrate; (a, b) as-synthesized SnO_2 powders after sintering, (c) bare SnO_2 photoanode, and (d) quantum dot-sensitized SnO_2-HMS photoanode.

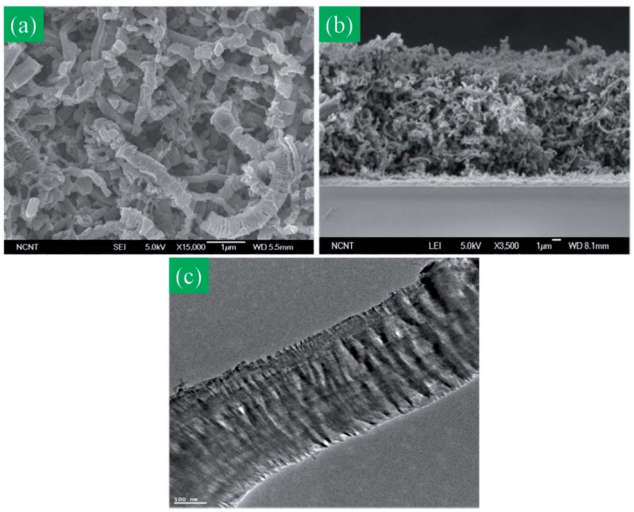

Fig. 3 SEM images of the CNF electrodes (a) top view of CNF on FTO glass substrates, (b) cross-sectional images of the CNF on FTO glass substrates, and (c) HR-TEM images of CNF powders.

results, mesoporous spherical TiO_2 (similar with SnO_2-HMS) were used as photoanode and exhibit better functionality for light reflectance when compared to nanoparticulate TiO_2 electrodes.[40] Such property is quite advantageous for photovoltaic applications. So our microspheres can function as scattering centers and the SnO_2-HMS can effectively confine visible light (400–750 nm) (Fig. S2†). We concluded that high reflectance of the SnO_2 nanostructure can enhance light harvesting and efficiency. Inset (Fig. S2†) shows the absorption spectra of QD-sensitized SnO_2-HMS photoelectrodes. After the sensitization of SnO_2-HMS with QDs (CdS/CdSe/ZnS), reflectance is reduced at the short wavelength range (under 650 nm) due to absorption of the incident light by the QDs.

Photocurrent–voltage characteristics of the QDSCs and DSCs with SnO_2 photoanode were assembled with either CNF or Pt CEs and their spectra are shown in Fig. 4a and b and their corresponding photovoltaic parameters are summarized in Table 1. To reduce the electron recombination and trap states at the SnO_2/CdS/CdSe/electrolyte interface or dye/electrolyte interface, an aqueous $TiCl_4$ treatment was done before the QD or dye-sensitization, and additionally a thin ZnS passivation layer was deposited on top of the CdS/CdSe by a SILAR method for QDSCs alone.[16]

When the CNF film was used as a CE, the QDSC exhibits a short circuit current (J_{sc}) of 7.5 mA cm^{-2}, an open circuit voltage (V_{oc}) of 0.587 V, a FF of 56.2%, and a power conversion efficiency (η) of 2.5%, which is quite superior to the conventional Pt CE (2.1%). Nanoparticulate TiO_2 electrodes were prepared for both QDSC and DSCs in similar SnO_2 experimental conditions with either CNF or Pt counter electrodes simultaneously. The device assembled with CNF CE showed a similar conversion efficiency to Pt for both the QDSC (Pt-2.0%, CNF-2.1%) and DSCs (Pt-7.4%, CNF-6.9%) and their photovoltaic parameters are summarized in Table S1.† Due to the lower conduction band of SnO_2 electrode, efficient charge injection from excited CdS/CdSe to the conduction band of SnO_2 was observed and so this

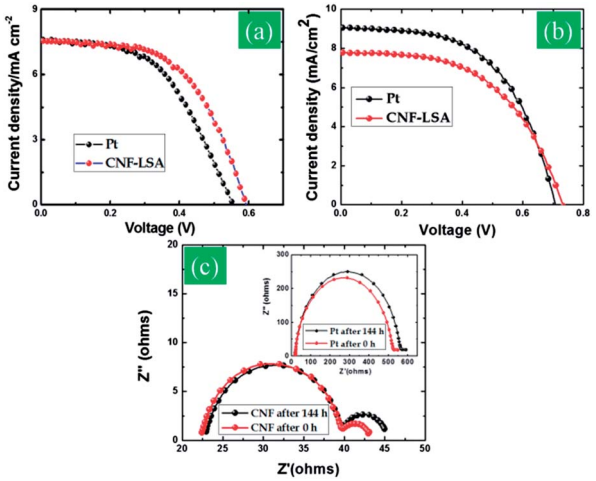

Fig. 4 (a) Current–voltage characteristics of QDSCs made with CNF and Pt CE, (b) current–voltage characteristics of DSCs made with CNF and Pt CE, and (c) Nyquist plots of the symmetric cells with CNF electrodes in polysulfide electrolyte with different aging times. Inset shows the corresponding characteristics of Pt CE in polysulfide electrolyte with different aging times.

Table 1 Photovoltaic performance of SnO_2-HMS photoanode for QDSCs and DSCs made with various counter electrodes. Measurement under 1 sun illumination

Counter electrode	Sensitizer	J_{sc} (mA cm^{-2})	V_{oc} (V)	FF (%)	η (%)
CNF	CdS/CdSe/ZnS QDs	7.5	0.587	56.2	2.5
Pt	CdS/CdSe/ZnS QDs	7.6	0.551	51.4	2.1
CNF	N719 dye	7.8	0.733	53.3	3.0
Pt	N719 dye	9.0	0.709	55.6	3.6

property allows us to use SnO_2 ahead of the standard TiO_2 electrodes.[16] With the addition of TiO_2 passivation layer on SnO_2, the sensitized QD can also act as a barrier layer for electron recombination back to the electrolyte and thus result in promising efficiency. The device assembled with CNF CE showed almost similar J_{sc} with the reference Pt CE device but much higher FF and V_{oc} than the Pt CE. Such enhanced performance originated from the much faster reduction reaction (S^{2-}/S_X^{2-}) in CNF CE. FF is mainly dependent upon the catalytic property of the counter electrode. The high surface area of CNF and catalytic rich region in the edges of the fibers decrease the charge transfer resistance (R_{CT}) in the CE and in turn increase the FF and η. The enhanced performance of CNF CE and poor catalytic property of Pt are estimated from the impedance analysis, as shown in Fig. 4c. Although the performance of SnO_2/CNF CE in QDSC is encouraging, it is still less than the reported value.[16] We believe there is still hope for efficiency improvement by controlling the QD deposition condition and optimizing the electrolyte composition. To further study the influence of SnO_2-HMS nanostructure, dye-sensitized solar cells were made simultaneously. In dye-sensitized SnO_2-HMS photoanode, CNF or Pt CE was used as a CE and iodine electrolyte acts as a redox mediator (Fig. 4b). Due to the high surface area, good porosity and hollow nanostructure, a large amount of dye molecules can be attached and the hollow structure can influence light scattering, faster electron transport route and all these properties resulted in a much promising photovoltaic performance in DSCs (3.6% for Pt CE, and 3.0% for CNF CE).

To study the interfacial catalytic reduction reaction in Pt and CNF CE with different aging times, electrochemical impedance spectroscopy (EIS) was performed (Fig. 4c). Thin layer symmetric cells were configured with the CNF coated FTO glass substrates, filled with polysulfide electrolyte, and simultaneously similar cells were prepared with the Pt for comparison.[34,36] In the Nyquist plot high frequency semicircle represent the charge transfer resistance (R_{CT}) in the CNF or Pt CE, an index of the catalytic property of the CE in QDSCs and DSCs, and the low frequency semicircle is from the Nernst diffusion impedance in the redox electrolyte.[33,36] Nyquist plots obtained from the CNF CE showed two distinguishing semicircles (Fig. 4c) and Pt showed one huge semicircle for R_{CT} and a small circle for a diffusion impedance (inset image of Fig. 4c). The R_{CT} for the Pt cell is about 20 times larger than CNF cell. This shows that the catalytic activity of CNF is much better than Pt. It may be reasonable to attribute such large overall impedance for Pt to the poor catalytic reduction reaction of Pt in the polysulfide electrolyte.[41] A key issue in using an alternative counter electrode in QDSCs is the robustness of the CE material in polysulfide electrolyte during aging.

The R_{CT} of freshly prepared CNF symmetric cells were found to be 23.2 Ω even after aging for 144 h, not a big difference, whereas symmetric cells made with the Pt showed a huge increase in the total impedance for 0 h and 144 h. Such increase in the impedance for Pt might have been due to adsorption of sulfur, which resulted in a larger impedance from the poor stability of the device. The poor catalytic activity of the Pt CE leads to a poor reduction rate of S_X^{2-}, which in turn leads to depletion of S^{2-} in the photoanode and inhibits QD regeneration and electron injection.[33,42]

To further evaluate the catalytic property of the CEs (CNF, Pt), Tafel-polarization was measured in a symmetric cell similar to the one used in EIS analysis.[43–45] Fig. 5a shows a plot of the logarithmic current density (log J) as a function of the voltage (V). Fig. 5a shows the anodic and cathodic branches of the Tafel curves for both CNF and Pt cells. Both the anodic and cathodic curves of CNF exhibit the largest slope than that of the Pt electrode. CNF electrodes have a higher exchange current density (J_o) towards polysulfide redox electrolyte compared to Pt. Hence, the CNF-CE shows the better electrocatalytic activity and is consistent with the EIS results.

To elucidate the results more clearly, cyclic voltammetry (CV) was also performed for the CNF and Pt electrodes (Fig. 5b). Here, CV was measured with a standard three electrode system composed of a working electrode, counter electrode and reference electrode. In the CV curves, the peak obtained on the positive side is known as anodic peak (oxidation of S^{2-}) and the peak obtained at the negative side is known as cathodic peak (reduction of S_X^{2-} to S^{2-}), respectively.[36,43] In the study of

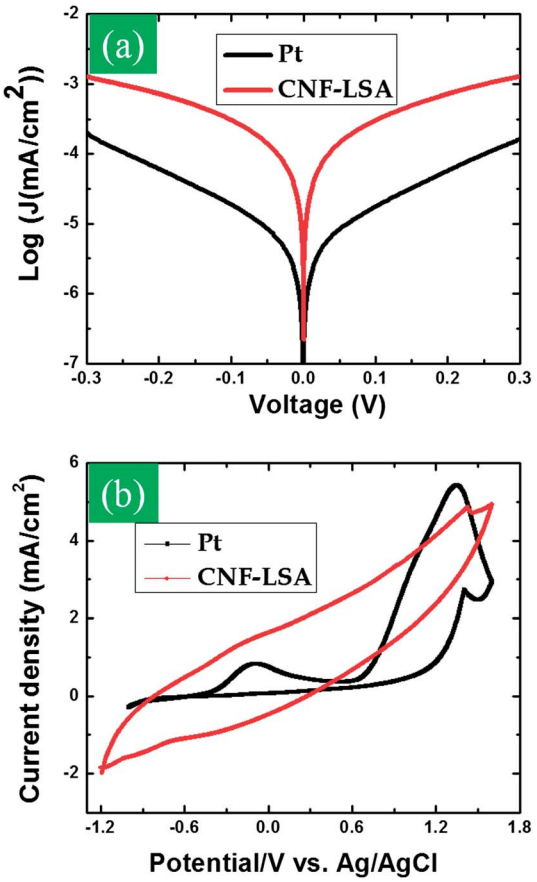

Fig. 5 (a) Tafel curves of the symmetric cells with CNF and Pt cells in polysulfide electrolyte. (b) Cyclic voltammograms for CNF, and Pt electrodes obtained at a scan rate of 50 mVs^{-1} in 1 mM Na_2S, 10 mM S aqueous solution containing 0.1 M $LiClO_4$ as supporting electrolyte.

counter electrodes, the reduction peak current was the most relevant, expressing the catalytic ability of counter electrode for S_X^{2-} reduction. Fig. 5b shows that a typical pair of redox peaks is observed for the CNF and Pt electrodes. In the cathodic peak, the current density of Pt is slightly higher than the CNF electrode, but has an insignificant effect on the catalytic performance. On the other hand, the anodic peaks of the CNF show higher current density than Pt, which has a direct influence on the catalytic and photovoltaic performance. Such enhanced catalytic properties arise from the larger active surface area and defect rich edge planes of CNF electrodes. All electrochemical studies (EIS, Tafel-polarization, and CV) are in good agreement with each other.

4. Conclusions

In this paper, we demonstrated sensitized solar cells made with cauliflower-like hollow SnO_2 photoanode sandwiched with the stable CNF CE showing a power conversion efficiency of 2.5% in QDSCs and 3.0% for DSCs, which is quite promising with the standard Pt CE (QDSCs: 2.1%, and DSCs: 3.6%). They are likely attributed to the high internal surface area and light scattering in between the microspheres and shell layers of hollow SnO_2 with CNF CE showing good electrocatalytic properties. The described chemical and structural methodology can be expected to manufacture stable and low-cost sensitized solar cells.

Acknowledgements

This work was financially supported by the World Class University program (Grant R31-2008-000-10059-0) and the National Research Laboratory project (Grant no. NRF-2010-0018087) through the National Research Foundation (NRF) of Korea funded by the Ministry of Education, Science and Technology.

References

1 B. O'Regan and M. Grätzel, *Nature*, 1991, **353**, 737–740.
2 P. Wang, S. M. Zakeeruddin, P. Comte, I. Exnar and M. Grätzel, *J. Am. Chem. Soc.*, 2003, **125**, 1166–1167.
3 A. Yella, H. W. Lee, H. N. Tsao, C. Yi, A. K. Chandiran, M. K. Nazeeruddin, E. W. G. Diau, C. Y. Yeh, S. M. Zakeeruddin and M. Grätzel, *Science*, 2011, **334**, 629–634.
4 A. J. Nozik, *Phys. E*, 2002, **14**, 115–120.
5 P. V. Kamat, *J. Phys. Chem. C*, 2008, **112**, 18737–18753.
6 W. W. Yu, L. Qu, W. Guo and X. Peng, *Chem. Mater.*, 2003, **15**, 2854–2860.
7 A. Kongkanand, K. Tvrdy, K. Takechim, M. Kuno and P. V. Kamat, *J. Am. Chem. Soc.*, 2008, **130**, 4007–4015.
8 T. Toyoda and Q. Shen, *J. Phys. Chem. Lett.*, 2012, **3**, 1885–1893.
9 E. Hendry, M. Koeberg, B. O'Regan and M. Bonn, *Nano Lett.*, 2006, **6**, 755–759.
10 K. Zhu, N. R. Neale, A. Miedaner and A. J. Frank, *Nano Lett.*, 2007, **7**, 69–74.
11 E. Ramasamy and J. W. Lee, *J. Phys. Chem. C*, 2010, **114**, 22032–22037.
12 S. H. Ko, D. Lee, H. W. Kang, K. H. Nam, J. Y. Yeo, S. J. Hong, C. P. Grigoropoulos and H. J. Sung, *Nano Lett.*, 2011, **11**, 666–671.
13 K. Sayama, H. Sugihara and H. Arakawa, *Chem. Mater.*, 1998, **10**, 3825–3832.
14 S. S. Shin, J. S. Kim, J. H. Suk, K. D. Lee, D. W. Kim, J. H. Park, I. S. Cho, K. S. Hong and J. Y. Kim, *ACS Nano*, 2013, **7**, 1027–1035.
15 B. Tan, E. Toman, Y. Li and Y. Wu, *J. Am. Chem. Soc.*, 2007, **129**, 4162–4163.
16 Md. A. Hossain, J. R. Jennings, Z. Y. Koh and Q. Wang, *ACS Nano*, 2011, **4**, 3172–3181.
17 Z. M. Jarzebski and J. P. Marton, *J. Electrochem. Soc.*, 1976, **123**, 299C–310C.
18 S. H. Ahn, D. J. Kim, W. S. Chi and J. H. Kim, *Adv. Mater.*, 2013, **25**, 4893–4897.
19 J. Liu, T. Luo, S. Mouli, F. Meng, B. Sun, M. Li and J. Liu, *Chem. Commun.*, 2010, **46**, 472–474.
20 M. Law, L. E. Greene, J. C. Johnson, R. Saykally and P. Yang, *Nat. Mater.*, 2005, **4**, 455–459.

21 O. K. Varghese, M. Paulose and C. A. Grimes, *Nat. Nanotechnol.*, 2009, **9**, 592–597.
22 Q. Huang, F. Li, Y. Gond, J. Luo, S. Yang, Y. Luo, D. Li, X. Bai and Q. Meng, *J. Phys. Chem. C*, 2013, **117**, 10965–10973.
23 H. J. Koo, Y. J. Kim, Y. H. Lee, W. I. Lee, K. Kim and N. G. Park, *Adv. Mater.*, 2008, **20**, 195–199.
24 J. Qian, P. Liu, Y. Xiao, Y. Jiang, Y. Cao, X. Ai and H. Yang, *Adv. Mater.*, 2009, **21**, 3663–3667.
25 E.-H. Kong, J. Lim, Y. Chang, Y.-H. Yoon, T. Park and H. M. Jang, *Adv. Energy Mater.*, 2013, **3**, 1344–1350.
26 J. A. Chang, J. H. Rhee, S. H. Im, Y. H. Lee, H. J. Kim, S. I. Seok, M. K. Nazeeruddin and M. Grätzel, *Nano Lett.*, 2010, **10**, 2609–2612.
27 J. Y. Chang, L. F. Su, C. H. Li, C. C. Chang and J. M. Lin, *Chem. Commun.*, 2012, **48**, 4848–4850.
28 M. A. Hossain, G. Yang, M. Parameswaran, J. R. Jennings and Q. Wang, *J. Phys. Chem. C*, 2010, **114**, 21878–21884.
29 Y. Tachibana, H. Y. Akiyama, Y. Ohtsuka, T. Torimoto and S. Kuwabata, *Chem. Lett.*, 2007, 88–89.
30 Z. Yang, C. Y. Chen, C. W. Liu, C. L. Li and H. T. Chang, *Adv. Energy Mater.*, 2011, **1**, 259–264.
31 Z. Yang, C. Y. Chen, C. W. Liu and H. T. Chang, *Chem. Commun.*, 2010, **46**, 5485–5487.
32 P. K. Santra and P. V. Kamat, *J. Am. Chem. Soc.*, 2012, **134**, 2508–2511.
33 P. Sudhagar, E. Ramasamy, W. H. Cho, J. W. Lee and Y. S. Kang, *Electrochem. Commun.*, 2011, **13**, 34–37.
34 V. Ganapathy, B. Karunagaran and S. W. Rhee, *ACS Appl. Mater. Interfaces*, 2011, **3**, 857–862.
35 E. Ramasamy, W. J. Lee, D. Y. Lee and J. S. Song, *Appl. Phys. Lett.*, 2007, **90**, 173103–173113.
36 V. Ganapathy, W. Kwon and S. W. Rhee, *J. Power Sources*, 2011, **196**, 10798–10805.
37 H. M. Pathan and C. D. Lokhande, *Bull. Mater. Sci.*, 2004, **27**, 85–111.
38 E.-H. Kong, Y.-J. Chang, Y.-C. Park, Y.-H. Yoon, H.-J. Park and H. M. Jang, *Phys. Chem. Chem. Phys.*, 2012, **14**, 4620–4625.
39 H. X. yang, J. F. Qian, Z. X. Chen, X. P. Ai and Y. L. Cao, *J. Phys. Chem. C*, 2007, **111**, 14067–14071.
40 Y.-C. Park, E.-H. Kong, Y.-J. Chang, B.-G. Kum and H. M. Jang, *Electrochim. Acta*, 2011, **56**, 7371–7376.
41 I. M. Sero, S. Gimenez, F. F. Santiago, R. Gomez, Q. Shen, T. Toyoda and J. Bisquert, *Acc. Chem. Res.*, 2009, **42**, 1848–1857.
42 Y.-L. Lee and Y.-S. Lo, *Adv. Funct. Mater.*, 2009, **19**, 604–609.
43 J. Dong, S. Jia, J. Chen, B. Li, J. Zheng, J. Zhao, Z. Wang and Z. Zhu, *J. Mater. Chem.*, 2012, **22**, 9745–9750.
44 X. Zeng, D. Xiong, W. Zhang, L. Ming, Z. Xu, Z. Huang, M. Wang, W. Chen and Y. B. Cheng, *Nanoscale*, 2013, **5**, 6992–6998.
45 G. Hodes, J. Manassen and D. Cahen, *J. Electrochem. Soc.*, 1980, **127**, 544–549.